The effect of Barium substitution on the structural and dielectric properties of $Pb_{1-x}Ba_x(Zr_{0.52}Ti_{0.43}(Al_{0.5}Sb_{0.5})_{0.05})O_3$ ceramics at the morphotropic phase boundary

A. Benmakhlouf[a,*], R. Makhloufi[a], A. Boutarfaia[a], B. Messai[a], F. Hadji[b], M. Nouiri[c]
[a]*Laboratory of Applied Chemistry (LCA), Matter Science Department, Mohamed Khider University, P.O. Box 145, 07000, Biskra, Algeria*
[b]*Laboratory of Molecular Chemistry and Environment (LMCE), Matter Science Department, Mohamed Khider University, P.O. Box 145, 07000, Biskra, Algeria*
[c]*Laboratory of Physics of Materials and Nanomaterials Applied in Environment (LaPhyMNE), Faculty of Sciences, University of Gabes, Gabes, Tunisia*

In this study PZT type ceramics with a general formula $Pb_{1-x}Ba_x(Zr_{0.52}Ti_{0.43}(Al_{0.5}Sb_{0.5})_{0.05})O_3$ where (x = 0.00, 0.04, and 0.08) were elaborated by the solid-state reaction and studied for their structural and dielectric properties in the region of the morphotropic phase boundary (MPB). Different techniques were used to characterize the obtained samples such as X-ray diffraction (XRD) which shows that the results confirm the high purity of prepared samples without any secondary phase and also indicate the coexistence of both the tetragonal and rhombohedral phases. All the absorption bands corresponding to the perovskite structure are exhibited by The Fourier Transform Infrared spectroscopy (FTIR). The scanning electronic microscopy (SEM) shows that the mean grain size was found between 2,84 and 2,14 µm, the Curie temperature (TC) decreased with increasing Ba^{2+} content. Furthermore, the effect of the temperature, frequency, and composition on the dielectric properties demonstrated a maximum value of the dielectric constant ε max = 38800 at 1 kHz when X= 0.08.

(Received March 6, 2023; Accepted May 19, 2023)

Keywords: PZT, Curie temperature, Structural, Morphotropic phase boundary, Dielectric properties.

1. Introduction

Lead zirconate titanate (PZT) materials were exploited in many fields of technology for commercial electronic applications such as sensors, actuators, and memories [1-3], due to their high dielectric and piezoelectric capabilities [4-6]. The adaptable PZT properties have not yet been adequately replaced; because of those responses occur close to the Morphotropic Phase Boundary (MPB) [7-9]. Perovskite type-oxide (ABO_3) involving $Pb(Zr_xTi_{1-x})O_3$ where Pb^{2+} ion occupied the A-site while Zr^{4+} and Ti^{4+} ions were accommodated at the B-site [8, 10]. Several studies [11, 12] have reported that the substitution effect regardless of the A and/or B site is an effective method to enhance the dielectric properties. The dopants can be classified into three categories [8, 13], the isovalent dopants such as (Ba^{2+}) [14] and (Sr^{+2}) [15], donor dopants (Sb^{+5}) [16], and acceptor dopants (Al^{+3}) [17], the category that attracts us is the isovalent dopants (Ba^{2+}) because of their effect on dielectric properties, where they can reduce the curie points and increase the dielectric constant [8], as well as avoiding the pyrochlore composition in perovskite structure [18]. This is what prompted some studies to investigate the barium impact substitution into PZT ceramics' dielectric properties [14, 19, 20]. Xiucai Wang et al. [21] found that the Ba^{2+} ion doping into PZT ceramics shows a very interesting effect on the dielectric properties and decreases the curie temperature from 85 to 48°C. The same tendency has been found by Dipti et al. [22] and Neha et al. [11] when Ba^{2+} ions were incorporated into the PZT system.

Therefore, in this work, we are trying to find stable and reproducible characteristics of PZT ceramics in the region of the morphotropic phase boundary, using the solid-state reaction

*Corresponding author: aymen.benmakhlouf@univ-biskra.dz
https://doi.org/10.15251/JOR.2023.193.295

known as ceramic, a sequence of compositions $Pb_{1-x}Ba_x(Zr_{0.52}Ti_{0.43}(Al_{0.5}Sb_{0.5})_{0.05})O_3$ (PBZTAS) were x=0.00, 0.04, and 0.08 were created. We attempt to study the effect of Barium substitutions on structural, microstructure, and dielectric properties.

2. Experimental part

2.1. Samples preparation

A series of $Pb_{1-x}Ba_x(Zr_{0.52}Ti_{0.43}(Al_{0.5}Sb_{0.5})_{0.05})O_3$ with (x = 0.00, 0.04, and 0.08) compositions were elaborated through the solid-state reaction [23] using oxide powders of PbO, $BaCO_3$, ZrO_2, TiO_2, and Al_2O_3 (99.00% purity, BIOCHEM) and Sb_2O_5 (99.998% purity, Alfa Aesar). To produce a high-quality homogenized powder, the reagents were dispersed in acetone under a magnetic stirring for 2 hrs, after drying; the well-combined powders were ground for 6 hrs in the air by using a mortar and pestle. After grinding, the final homogenized powders were put in alumina crucibles and then calcined at 1000 °C for 2hrs with a heating rate of 2 °C/min, then manually reground for 2hrs. The obtained powders were mixed with 5% by weight of polyvinyl alcohol as a binder before being compacted into disk-shaped specimens and pressed into cylindrical pellets of 10 mm diameter and about 3 mm height by pressing at 1 ton/cm2 for 5 min by a hydraulic uniaxial press. Thereafter, to compact the pellet and reduce the porosity, the pellets were sintered at several temperatures (1190, 1210, 1230, 1250, and 1270 °C) for 2 hrs, with the same heating rate. To avoid lead loss during the sintering process and improve the density, lead zirconate (PZ) should be added [10, 24].

2.2. Samples characterization

The identification of phases and structural properties of the prepared samples were performed by X-ray diffraction analysis using (Rigaku Miniflex 600) type diffractometer with Cu-Kα (λ=1.5406 Å) radiation source. The Bragg's angle (2θ) has been scanned from 10° to 90° with a scanning rate of 0.04°/sec at room temperature. The surface morphology of the sintered pellets has been examined by scanning electron microscopy (TESCAN VEGA3), and the pellets samples were scanned under a high-resolution field emission gun SEM. The Fourier Transform Infrared spectroscopy (FTIR) of the samples was carried out on a PerkinElmer FT-IR Spectrum Two spectrophotometer in the wavelength range of 400–1500 cm^{-1}. The dielectric measurements were implemented by using a Wayne-Kerr 6425 analyzer component over the frequency range of 1-1000 kHz and a temperature interval ranging between 300 and 700 K. To improve the conductivity of the pellets, it's necessary to paint them with a high-purity silver paste and dried at 423K in an oven for 4 hrs, then we let them cool at room temperature [25].

3. Results and discussion

3.1. Structural properties

Figure 1 presents the XRD patterns of the analyzed samples calcined at 1000 °C for 2hrs as a function of different barium content (Ba^{2+}) as a dopant. XRD peaks corresponding to each sample have been superposed to those of the crystallographic database namely ICDD-PDF2.

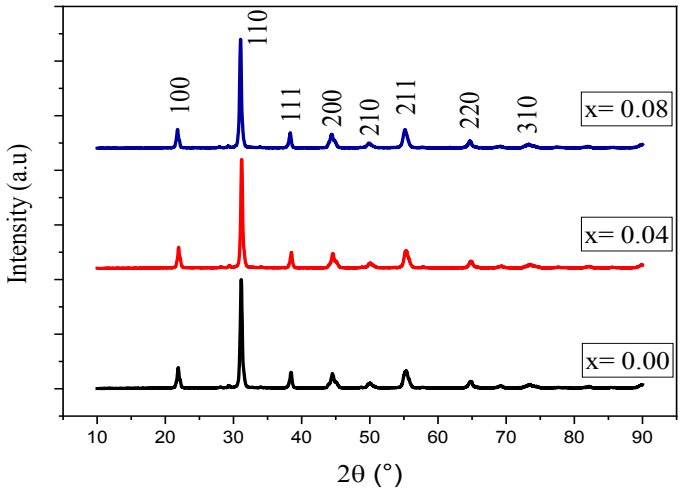

Fig. 1. XRD patterns of $Pb_{1-X}Ba_X(Zr_{0.52}Ti_{0.43}(Al_{0.5}Sb_{0.5})_{0.05})O_3$.

We found that a perovskite structure was successfully formed for each composition studied without any detectable secondary phase, indicating that the Ba^{2+} ions are well incorporated in the crystal lattice.

Figure 2 shows the deconvoluted peak situated between 42° and 47° by using the Gaussian function which helps us to observe three small peaks corresponding to the (002) and (200) of Tetragonal phase (T) and (200) of the Rhombohedral phase (R), suggesting the coexistence of two phases T+R at the same time, meaning that we are in the region of the MPB [26], this is what prompted us to evaluate the fraction of the two tetragonal (F_T) and rhombohedral (F_R) phases by estimating the relative intensities of the deconvoluted peaks T(002), T(200), and R(200), using the following equations [27-29]:

$$F_T\,(\%) = \frac{I_{(002)T}+I_{(200)T}}{I_{(002)T}+I_{(200)T}+I_{(200)R}} * 100 \quad (1)$$

$$F_R\,(\%) = 100 - F_T\,(\%) \quad (2)$$

in which $I_{(002)T}$, $I_{(200)T}$, and $I_{(002)R}$ are the integrated area of Tetragonal (002), Tetragonal (200), and Rhombohedral (200) peaks, respectively, the obtained data are illustrated in figure 2.

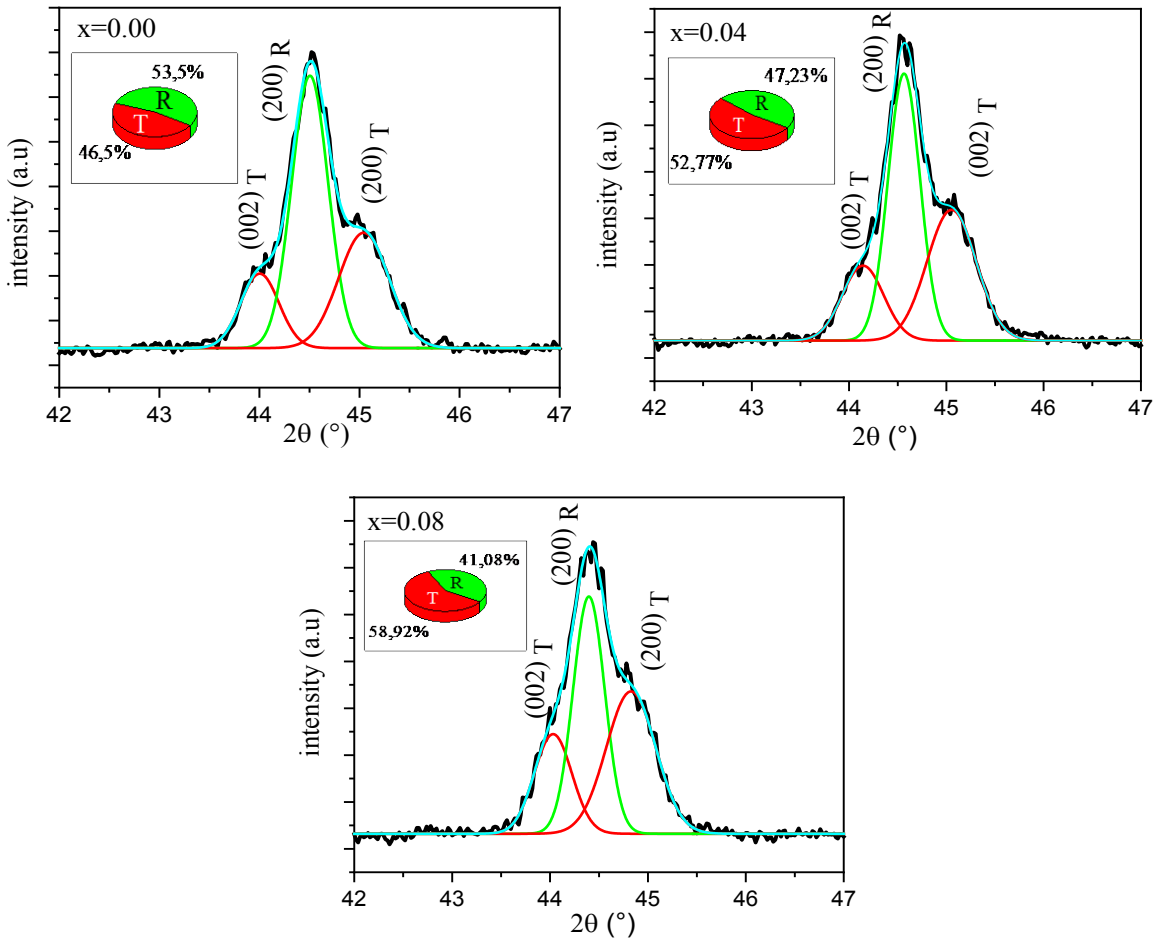

Fig. 2. The deconvoluted peaks simulated in 2θ range of 42° to 47° and the volume fraction of the Tetragonal (T) and Rhombohedral (R) phases of $Pb_{1-X}Ba_X(Zr_{0.52}\,Ti_{0.43}(Al_{0.5}\,Sb_{0.5})_{0.05})O_3$.

The c/a ratio represents the tetragonality of the specimens prepared [30], which increases with the increase of Ba^{2+} ion amount, the rise of tetragonality suggesting that the substitution of Ba^{2+} ion could be preferred the formation of the tetragonal phase rather than the rhombohedral phase. The crystallite size was calculated using the Debye-Scherer formula [31, 32]:

$$D=\frac{0.9\lambda}{\beta\cos\theta} \tag{3}$$

where D is the size of the crystallites, λ= 1.5406 Å represents the wavelength of CuKa X-ray, θ is the half angle of Bragg in degrees, β means the full width at half-maximum (FWHM), the results were showing in table 1. The crystallite size increase with increasing of Ba^{2+} content due to the difference between the ionic sizes of Ba^{2+} (1.61 Å) and Pb^{2+} (1.49 Å) [33]. Moreover, the tolerance factor (T) is a term in which we can evaluate the stability of the perovskite structure using the following equation [34]:

$$T=\frac{R_A+R_O}{\sqrt{2}(R_B+R_O)} \tag{4}$$

in which R_A, R_B, and R_O are the ionic radii of the A-site, B-site, and oxygen atoms, respectively. Where the ionic radii of Pb^{2+}, Ba^{2+}, Zr^{4+}, Ti^{4+}, Sb^{5+}, Al^{3+}, and O^{2-} are 1.49, 1.61, 0.72, 0.605, 0.62, 0.54, and 1.35 Å, respectively [21, 35, 36]. The calculated values of T are listed in Table 1, the results of the tolerance factor are in the range of 0.9968 and 1.0001 which indicates the stability of

the perovskite structure[37], in addition, the increase of Ba^{+2} amounts brings the tolerance factor close to 1, which makes the perovskite structure more stable[38].

Table 1. The lattice parameters, c/a ratio, tolerance factor T, and the crystallite size of $Pb_{1-X}Ba_X(Zr_{0.52}Ti_{0.43}(Al_{0.5}Sb_{0.5})_{0.05})O_3$.

Samples	T	crystallite size (nm)	Lattice parameter		
			a (Å)	c (Å)	c/a
X= 0.00	0.9968	13,78	4.748	4.022	0,847
X= 0.04	0.9985	15,56	4.734	4.021	0,849
X= 0.08	1.0001	15,80	4.745	4.040	0,851

Several infrared absorption studies on perovskite have been carried out to evaluate the frequencies of the normal modes of vibration of these compositions [39, 40]. PZT-based materials have four vibration modes, two vibration modes which are located below 400 cm^{-1}, these two modes correspond to the vibrations in the Pb-TiO_3 or ZrO_3 bond, the third mode has a wavenumber range of 390 - 410 cm^{-1}, where it is caused by the stretching vibrations of O-Zr and Ti-O [41], these three modes can't be observed due to the measurement limitation of our equipment which begins measuring from 400 cm^{-1}, the fourth vibration mode is the most important band which is between 440 cm^{-1} and 640 cm^{-1}, it's characterized by the vibration of M-O (M= Zr, Ti, and Pb) octahedron asymmetrical stretching which is presented in figure 3 [42-44]. The FTIR results are consistent with the XRD results above and confirmed that the perovskite structure was successfully formed.

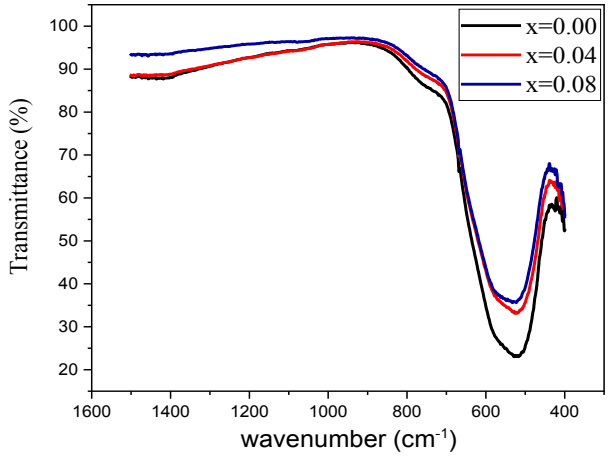

Fig. 3. FTIR patterns of $Pb_{1-x}Ba_x(Zr_{0,52}Ti_{0,43}(Al_{0,5}Sb_{0,5})_{0,05})O_3$.

3.2. Microstructural analysis

The best morphological properties of our samples are having a minimum of pores, more compact and dense; to obtain this type of samples it is necessary to find the optimal temperature of sintering. To determine this temperature, we sintered our samples with several temperatures between 1170°C to 1270°C with a step of 20°C. Figure 4 represents the variation of the density of different compositions doped by Ba^{+2} ion as a function of the sintering temperature, the best temperature of sintering is 1220°C which offers the densest samples with a density value of around 7.2 g/cm^3, this is a very favorable factor for excellent dielectric properties [45].

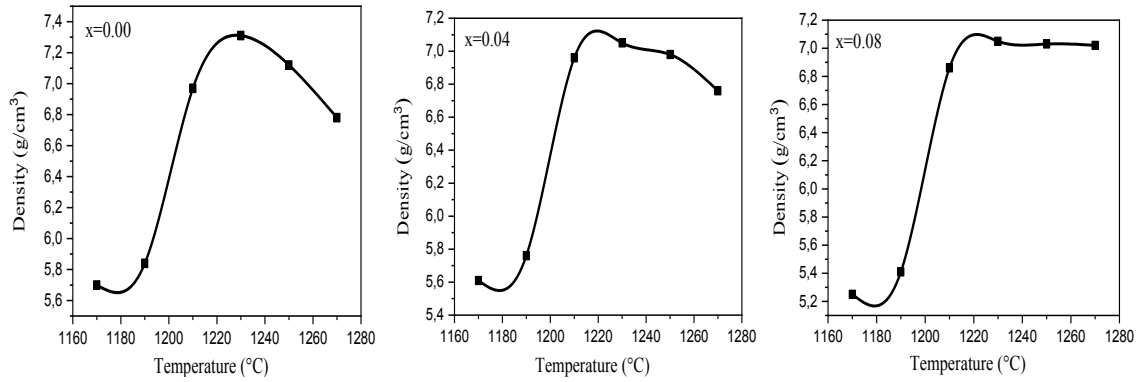

Fig. 4. Influence of the temperature on the density of $Pb_{1-X}Ba_X(Zr_{0.52}Ti_{0.43}(Al_{0.5}Sb_{0.5})_{0.05})O_3$.

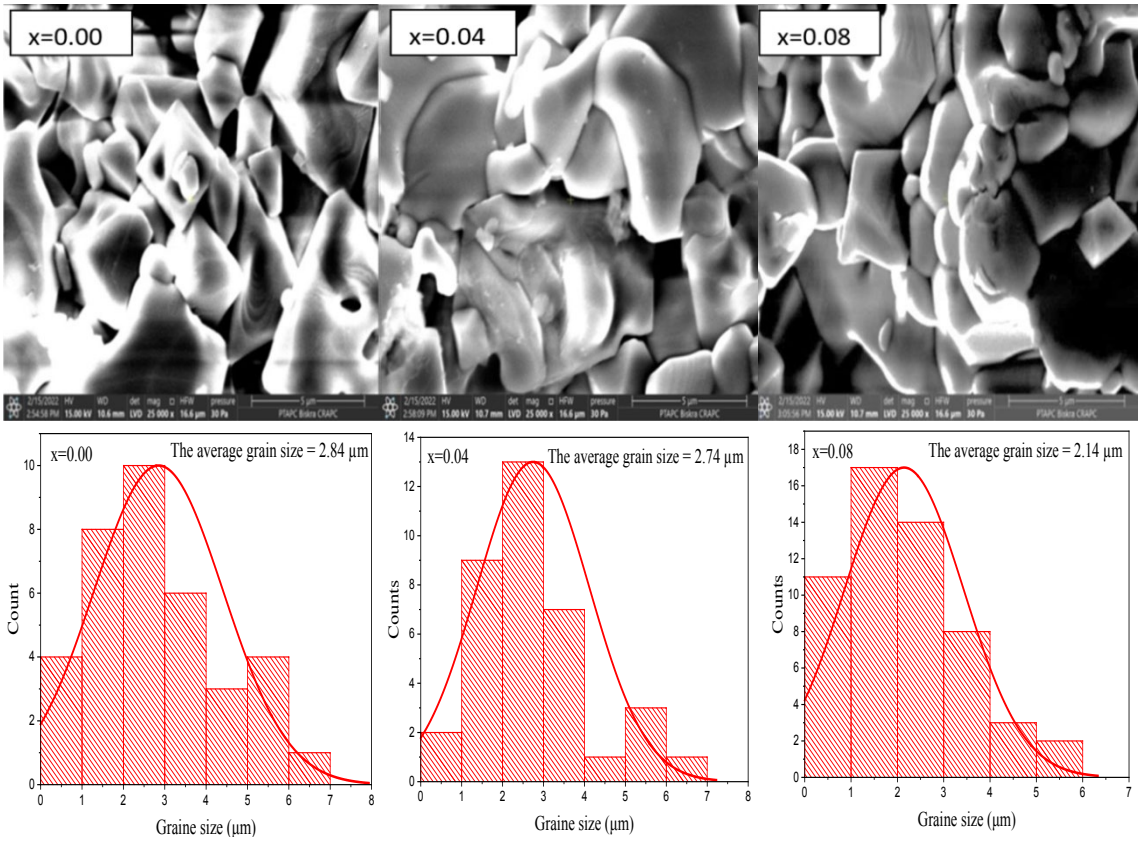

Fig. 5. SEM images of fracture surface and the average grain size of $Pb_{1-X}Ba_X(Zr_{0.52}Ti_{0.43}(Al_{0.5}Sb_{0.5})_{0.05})O_3$.

Figure 5 represents the SEM micrographs of the specimens sintered at 1220°C, it can be seen that the microstructure of the studied samples is dense and composed of grains having different shapes and relatively small sizes. Image J software was used to approximate the average grain size, it was noticed that the grain size of the compositions x = 0.00, 0.04, and 0.08 are found to be 2.84, 2.74, and 2.14 µm respectively. Indicating a reduction of the mean grain size with increasing of Ba^{+2} content, which could improve the dielectric constant [46].

3.3. Dielectric studies

To get an idea about the electrical properties of materials as a function of temperature and frequency, it's necessary to make the dielectric measurement. The two main electrical characteristics that we can take from the dielectric measurements are the capacity and the

conductivity, one which is related to the insulation of materials and the other which is related to the transport of electronic charge, and from this analysis, we can determine the constant and the dielectric loss [47]. The equation in which we can calculate the dielectric constant is the following [24, 32]:

$$\varepsilon_r = \frac{C_p * d}{\varepsilon_0 * A} \quad (5)$$

where C_p is the parallel capacitance, the thickness of the pellet is denoted by d, A is a ceramic disc area and ε_0 is the free space permittivity ($\varepsilon_0 = 8{,}85*10^{-12}$F/m).

Figure 6 represents the variation of the dielectric constant (ε_r) and dielectric loss (tgδ) of the $Pb_{1-X}Ba_X(Zr_{0,52}Ti_{0,43}(Al_{0,5}Sb_{0,5})_{0,05})O_3$ where x = 0.00, 0.04, and 0.08 sintered at 1220 °C as a function of temperature (300 K–700 K) at several selected frequencies (1, 2, 4, 6, 8, and 10 kHz), it can be seen that the dielectric constant gradually increases with the increase in temperature until the $\varepsilon_{r\,max}$ which corresponds to a specific temperature, after this temperature, the dielectric constant will be strongly decreased which indicate ferroelectric phase transition [48], the temperature where the phase change from ferroelectric to paraelectric (cubic structure) is called the Curie Temperature (TC) or the phase transition temperature [22].

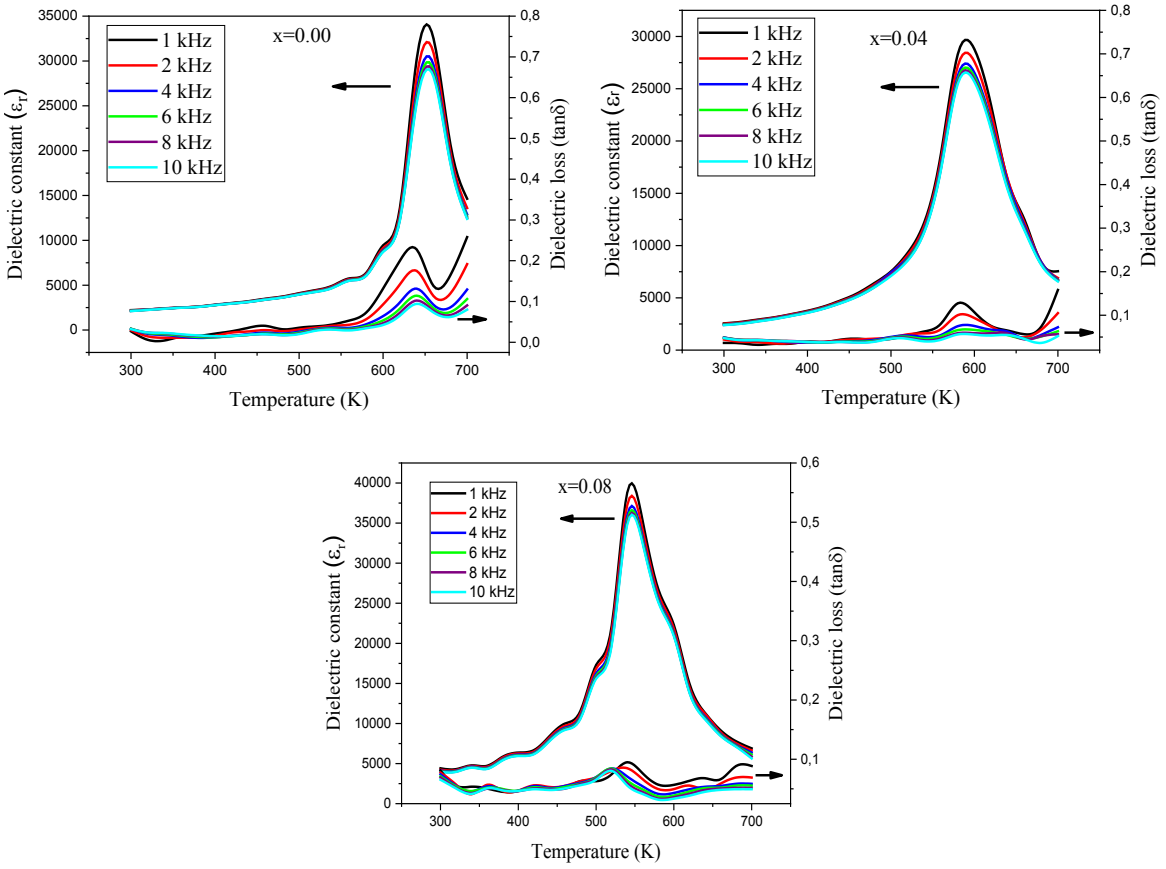

Fig. 6. Temperature dependence of Dielectric constant ε_r and Dielectric loss (tgδ) at different frequencies of $Pb_{1-X}Ba_X(Zr_{0.52}Ti_{0.43}(Al_{0.5}Sb_{0.5})_{0.05})O_3$.

The highest dielectric constant was found at the Curie temperature $\varepsilon_{max,}$ which is probably due to the thermally activated electrons in the system [49]. We can observe also that the curie temperature is not changing as a function of frequency, indicating the normal ferroelectric characteristics [50, 51]. In contrast, the substitution of the Ba^{2+} ion into the PZT system reduces

the curie temperature, most likely due to the interaction of the vacancies created by the Ba^{2+} ion and the reduction of the lattice vibrations [20, 52].

The dielectric constant ε_r drops with increasing frequency which is a general characterization of polar dielectric materials[53], which indicates the presence of all types of polarizations at the same time (dipole, ionic, space charge, electronics, etc.)[40, 54]. Concerning the dielectric loss (tgδ), which have very small values, there is decreasing with increasing frequency, also the increase in the dielectric loss at high temperatures could be assigned to the increase in conductivity [55]. the Curie temperature (TC), dielectric constant at curie temperature (ε_{max}), dielectric constant at room temperature (ε_{RT}), dielectric loss at curie temperature ($tg\delta_{Tc}$), dielectric loss at room temperature ($tg\delta_{RT}$) at a frequency of 1 kHz of PBZTAS with x = 0.00, 0.04, and 0.08 are listed in table 2.

Table 2. Variation of TC, $\varepsilon_{r\,RT}$, ε_{max}, $Tg\delta_{RT}$ and $Tg\delta_{Tc}$ of $Pb_{1-X}Ba_X(Zr_{0.52}Ti_{0.43}(Al_{0.5}Sb_{0.5})_{0.05})O_3$ at 1 kHz.

PBZTAS	TC	ε_{max}	$\varepsilon_{r\,RT}$	$Tg\delta_{TC}$	$Tg\delta_{RT}$
X= 0.00	660	32497	2219	0.138	0.268
X= 0.04	600	28787	2557	0.107	0.036
X= 0.08	540	38800	4407	0.095	0.081

Figure 7 shows the dielectric constant as a function of temperature at 1 kHz of $Pb_{1-X}Ba_X(Zr_{0.52}Ti_{0.43}(Al_{0.5}Sb_{0.5})_{0.05})O_3$. The compound which corresponds to the strongest dielectric response is that of x= 0.08 (ε_{max}= 38800) which is much higher compared to previous studies [11, 47, 50]. The broadening of the dielectric peaks and the variation of the maximum value of the dielectric constant $\varepsilon_{r\,max}$ with the addition of Ba^{+2} content resulting from the origin of grain size variation and structural disorder [56].

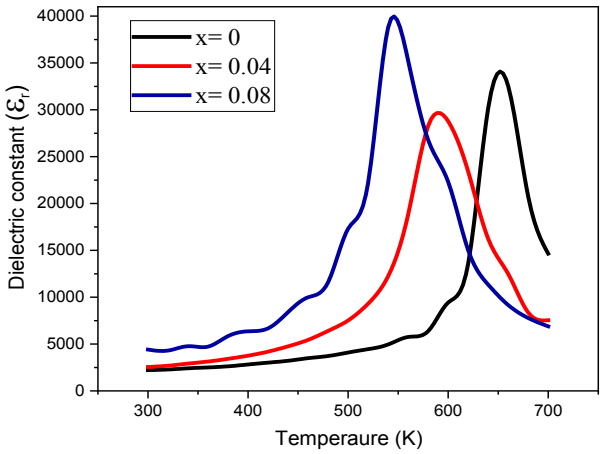

Fig. 7. Temperature dependence of Dielectric constant (ε_r) at 1 kHz of $Pb_{1-X}Ba_X(Zr_{0.52}Ti_{0.43}(Al_{0.5}Sb_{0.5})_{0.05})O_3$.

4. Conclusion

In this study, the $Pb_{1-X}Ba_X(Zr_{0,52}Ti_{0,43}(Al_{0,5}Sb_{0,5})_{0,05})O_3$ ceramics where (x = 0.00, 0.04, and 0.08) have been successfully prepared using the solid-state reaction, XRD patterns illustrate the coexistence of the tetragonal and rhombohedral phase without any secondary phases, which showing the morphotropic phase boundary. The addition of Ba^{2+} ion improves the stability of our perovskite structure; decreases the grain size; dropped the curie temperature from 660 °C to 540 °C; has an obvious effect on the dielectric constant, which increases it from 32497 corresponding

the undoped sample up to 38800 corresponding x=0.08 at the Curie temperature and frequency of 1 kHz.

Acknowledgements

The authors gratefully acknowledge the Directorate General of Scientific Research and Technological Development (DGRSDT), Algeria for funding the PhD project.

References

[1] S. Yan, C. Sun, Q. Cui, M. He, R. Wang, J. Hao, X. Chu, Mater. Chem. Phys. 255 (2020) 123605. https://doi.org/https://doi.org/10.2298/PAC1603175M.
[2] M.D. Durruthy-Rodríguez, J. Portellez-Rodríguez, J.F. Bentancourt, M. Hernández-García, M.A. Hernández-Landaverde, F. Rodríguez-Melgarejo, J.M. Yañez-Limón, Appl. Phys. A 127 (2021) 1-8. https://doi.org/https://doi.org/10.1007/s00339-021-04829-7.
[3] I. Abdulmajeeda, S. Ibraheemb, Journal of Ovonic Research 18 (2022) 499-505. https://doi.org/https://doi.org/10.15251/JOR.2022.184.499
[4] F. Guo, S. Zhang, W. Long, P. Fang, X. Li, Z. Xi, Ceram. Int. (2022). https://doi.org/https://doi.org/10.1016/j.ceramint.2022.04.308.
[5] H. Chen, T. Pu, S. Fan, H. Liu, J. Zhu, Q. Chen, Mater. Res. Bull. 146 (2022) 111576. https://doi.org/https://doi.org/10.1016/j.materresbull.2021.111576.
[6] T. Rashid, Z.A. Ahmad, H. Mohamad, J. Mater. Sci. - Mater. Electron. 32 (2021) 18095-18107. https://doi.org/https://doi.org/10.1007/s10854-021-06354-y.
[7] B. Tiwari, C. RNP, Int. Res. J. Adv. Sci. Hub 2 (2020) 44-48. https://doi.org/https://doi.org/10.47392/irjash.2020.146.
[8] P. Panda, B. Sahoo, Ferroelectrics 474 (2015) 128-143. https://doi.org/https://doi.org/10.1080/00150193.2015.997146.
[9] V. Pal, O. Thakur, R. Dwivedi, J. Phys. D: Appl. Phys. 48 (2015) 055301. https://doi.org/https://doi.org/10.1088/0022-3727/48/5/055301.
[10] S. Sen, R. Choudhary, A. Tarafdar, P. Pramanik, J. Appl. Phys. 99 (2006) 124114. https://doi.org/https://doi.org/10.1063/1.2206850.
[11] R. Pandey, M. Bhatnagar, P. Kumar, R.K. Malik, C. Prakash, Mater. Lett. 318 (2022) 132126. https://doi.org/https://doi.org/10.1016/j.matlet.2022.132126.
[12] Z. Huang, Y. Lai, W. Guan, Y. Zeng, Y. Wei, S. Wu, J. Han, Y. Mao, Y. Xiang, Mater. Lett. 178 (2016) 163-165. https://doi.org/https://doi.org/10.1016/j.matlet.2016.05.010.
[13] B. Sahoo, P.K. Panda, J. Mater. Sci. 42 (2007) 9684-9688. https://doi.org/https://doi.org/10.1007/s10853-007-1948-4.
[14] Z. Xu, X. Zeng, Z. Cao, L. Ling, P. Qiu, X. He, Ceram. Int. 45 (2019) 17890-17897. https://doi.org/https://doi.org/10.1016/j.ceramint.2019.06.005.
[15] K. Ramam, M. Lopez, Mater Sci Eng B 145 (2007) 41-47. https://doi.org/https://doi.org/10.1016/j.mseb.2007.09.085.
[16] L. Hamzioui, F. Kahoul, A. Boutarfaia, A. Guemache, M. Aillerie, Process. Appl. Ceram 14 (2020) 19-24. https://doi.org/https://doi.org/10.2298/PAC2001019H.
[17] R. Rai, S. Sharma, R. Choudhary, J. Mater. Sci. 41 (2006) 4259-4265. https://doi.org/https://doi.org/10.1007/s10853-005-5455-1.
[18] Q. Zhang, X. Liu, Y. Zhang, X. Song, J. Zhu, I. Baturin, J. Chen, Ceram. Int. 41 (2015) 3030-3035. https://doi.org/https://doi.org/10.1016/j.ceramint.2014.10.139. .
[19] B.P. Kumar, S. Sangawar, H. Kumar, Ceram. Int. 40 (2014) 3809-3812. https://doi.org/https://doi.org/10.1016/j.ceramint.2013.08.014.
[20] K. Ramam, M. Lopez, J. Phys. D: Appl. Phys. 39 (2006) 4466. https://doi.org/https://doi.org/10.1088/0022-3727/39/20/025.

[21] X. Wang, W. Cai, Z. Xiao, X. Yu, J. Chen, T. Yang, J. Mater. Sci. - Mater. Electron. 31 (2020) 17013-17017. https://doi.org/https://doi.org/10.1007/s10854-020-04258-x.
[22] J. Juneja, S. Singh, K. Raina, C. Prakash, Phys. B: Condens. Matter 431 (2013) 109-114. https://doi.org/https://doi.org/10.1016/j.physb.2013.09.011.
[23] F. Kahoul, L. Hamzioui, A. Guemache, M. Aillerie, A. Boutarfaia, J. Chem. Soc. Pak. 42 (2020). https://doi.org/https://doi.org/10.52568/000682/JCSP/42.05.2020.
[24] A. Kumar, V. Pal, S. Mishra, J. Mater. Sci. - Mater. Electron. 32 (2021) 2946-2952. https://doi.org/https://doi.org/10.1007/s10854-020-05046-3.
[25] R. Ranjan, R. Kumar, B. Behera, R. Choudhary, Mater. Chem. Phys. 115 (2009) 473-477. https://doi.org/https://doi.org/10.1016/j.matchemphys.2009.01.017.
[26] X. Huang, J. Zeng, X. Ruan, L. Zheng, G. Li, J. Am. Ceram. Soc. 101 (2018) 274-282. https://doi.org/https://doi.org/10.1111/jace.15179.
[27] Y. Luo, T. Pu, S. Fan, H. Liu, J. Zhu, J. Adv. Dielectr 12 (2022) 2250001. https://doi.org/https://dx.doi.org/10.1142/S2010135X22500011.
[28] C.-C. Tsai, S.-Y. Chu, J.-S. Jiang, C.-S. Hong, Y.-F. Chiu, Ceram. Int. 40 (2014) 11713-11725. https://doi.org/https://doi.org/10.1016/j.ceramint.2014.03.185.
[29] Z. Xia, Q. Li, Solid State Commun. 142 (2007) 323-328. https://doi.org/https://doi.org/10.1016/j.ssc.2007.03.004.
[30] K.M. Batoo, R. Verma, A. Chauhan, R. Kumar, M. Hadi, O.M. Aldossary, Y. Al-Douri, J. Alloys Compd. 883 (2021) 160836. https://doi.org/https://doi.org/10.1016/j.jallcom.2021.160836.
[31] M. Anupama, B. Rudraswamy, N. Dhananjaya, J. Alloys Compd. 706 (2017) 554-561. https://doi.org/https://doi.org/10.1016/j.jallcom.2017.02.241.
[32] A. Sharma, K.M. Batoo, O.M. Aldossary, S. Jindal, N. Aggarwal, G. Kumar, J. Mater. Sci. - Mater. Electron. 32 (2021) 313-322. https://doi.org/https://doi.org/10.1007/s10854-020-04782-w.
[33] P. Kour, P. Kumar, S. Sinha, M. Kar, Solid State Commun. 190 (2014) 33-39. https://doi.org/https://doi.org/10.1016/j.ssc.2014.03.025.
[34] Z. Dai, W. Liu, D. Lin, X. Ren, Mater. Lett. 215 (2018) 46-49. https://doi.org/https://doi.org/10.1016/j.matlet.2017.12.036.
[35] Q. Peng, W. Jin-Feng, M. Bao-Quan, W. Chun-Ming, L. Xing-Hua, Chin. Phys. Lett 24 (2007) 3535. https://doi.org/https://doi.org/10.1088/0256-307X/24/12/067.
[36] T.-F. Cao, J.-Q. Dai, X.-W. Wang, Ceram. Int. 46 (2020) 7954-7960. https://doi.org/https://doi.org/10.1016/j.ceramint.2019.12.016.
[37] A. Meklid, S.E. Hachani, Z. Necira, H. Menasra, M. Abba, A. Boutarfaia, Appl. Phys. A 126 (2020) 1-7. https://doi.org/https://doi.org/10.1007/s00339-019-3209-1.
[38] W.-C. Lee, C.-Y. Huang, L.-K. Tsao, Y.-C. Wu, J. Eur. Ceram. Soc. 29 (2009) 1443-1448. https://doi.org/https://doi.org/10.1016/j.jeurceramsoc.2008.08.028.
[39] C. Perry, B. Khanna, G. Rupprecht, Phys. Rev. 135 (1964) A408. https://doi.org/https://doi.org/10.1103/PhysRev.135.A408.
[40] S. Revathi, L.J. Kennedy, S. Basha, R. Padmanabhan, J. Nanosci. Nanotechnol 18 (2018) 4953-4962. https://doi.org/https://doi.org/10.1166/jnn.2018.15336.
[41] P. Kour, S. Pradhan, P. Kumar, S. Sinha, M. Kar, Mater. Today: Proc 4 (2017) 5727-5733. https://doi.org/https://doi.org/10.1016/j.matpr.2017.06.037.
[42] G. Pecchi, C. Campos, O. Peña, L.E. Cadus, J. Mol. Catal. A: Chem. 282 (2008) 158-166. https://doi.org/https://doi.org/10.1016/j.molcata.2007.12.022.
[43] D. Sun, X. Jin, H. Liu, J. Zhu, Y. Zhu, Y. Zhu, Ferroelectrics 355 (2007) 145-148. https://doi.org/https://doi.org/10.1080/00150190701517630.
[44] A. Mirzaei, M. Bonyani, S. Torkian, Process. Appl. Ceram 10 (2016) 175-182. https://doi.org/https://doi.org/10.2298/PAC1603175M.
[45] N. Zidi, A. Chaouchi, M. Rguiti, Y. Lorgouilloux, C. Courtois, J. Mater. Sci. - Mater. Electron. (2022) 1-20. https://doi.org/https://doi.org/10.1007/s10854-022-08369-5.
[46] P. Parjansri, U. Intatha, S. Eitssayeam, Mater. Res. Bull. 65 (2015) 61-67. https://doi.org/https://doi.org/10.1016/j.materresbull.2015.01.040.

[47] N. Sahu, S. Panigrahi, M. Kar, Ceram. Int. 38 (2012) 1549-1556. https://doi.org/https://doi.org/10.1016/j.ceramint.2011.09.040.
[48] D. Mahato, R. Chaudhary, S. Srivastava, J. Mater. Sci. 40 (2005) 381-386. https://doi.org/https://doi.org/10.1007/s10853-005-6094-2.
[49] M. Arshad, H. Du, M.S. Javed, A. Maqsood, I. Ashraf, S. Hussain, W. Ma, H. Ran, Ceram. Int. 46 (2020) 2238-2246. https://doi.org/https://doi.org/10.1016/j.ceramint.2019.09.208.
[50] P. Singh, S. Singh, J. Juneja, C. Prakash, Ceram. Int. 35 (2009) 3335-3338. https://doi.org/https://doi.org/10.1016/j.ceramint.2009.05.036.
[51] Y. Xu, Ferroelectric materials and their applications, Elsevier2013.
[52] K. Ramam, V. Miguel, EPJ Appl. Phys. 35 (2006) 43-47. https://doi.org/https://doi.org/10.1051/epjap:2006065.
[53] F. Kahoul, L. Hamzioui, A. Guemache, M. Aillerie, A. Boutarfaia, Ferroelectrics 572 (2021) 229-237. https://doi.org/https://doi.org/10.1080/00150193.2020.1868885.
[54] R. Ranjan, R. Kumar, R. Choudhary, Phys. Res. Int. 2009 (2009). https://doi.org/https://doi:10.1155/2009/382578.
[55] O. Thakur, C. Prakash, Ph. Transit. 76 (2003) 567-574. https://doi.org/https://doi.org/10.1080/01411590290030708.
[56] M.E. Lines, A.M. Glass, Principles and applications of ferroelectrics and related materials, Oxford university press2001.